



ELSEVIER

Nuclear Instruments and Methods in Physics Research A 457 (2001) 299–308

**NUCLEAR
INSTRUMENTS
& METHODS
IN PHYSICS
RESEARCH**
Section A

www.elsevier.nl/locate/nima

Monte Carlo simulation of crystal monochromators/analysers – Applications for the crystal-analyser neutron spectrometer IRIS

G. Zsigmond*, F. Mezei, D. Wechsler, F. Streffer

Hahn-Meitner-Institut Berlin, Glienicke Strasse 100 D-14109 Berlin, Germany

Received 24 May 2000; accepted 15 June 2000

Abstract

It is shown that Monte Carlo simulations of a crystal monochromator/analyser by means of the Virtual Instrumentation Tool for ESS (VITESS) offer a correct basis for the computation of the resolution function of crystal analyser spectrometers. Relying on comparisons of MC computed and measured data of vanadium and superfluid helium, a benchmarking of the programme codes of IRIS was performed practically limited only by the statistics of the experimental calibration data. Recent results from the study of the input time pulses from the liquid hydrogen moderator and pulse-shaping choppers are also mentioned. © 2001 Elsevier Science B.V. All rights reserved.

PACS: 29.30.Hs; 29.85.+c; 29.25.Dz

Keywords: Monte Carlo simulation; Neutron spectrometry; Neutron optics; Backscattering; Data analysis; Instrumentation

1. Introduction

Neutron scattering instruments are composed of several standard and/or non-standard neutron optics modules, starting with often complex guide and chopper systems up to collimators and focussing monochromators/analysers. Due to the beam divergence, for example, most of the neutrons are scattered multiple times in each component of the instrument. However, information on the single

neutron trajectories, flight times, scattering angles cannot be collected during an experiment.

Consequently, classical data reduction programmes handle the raw data output by considering a model of an ideal situation. As a collective measure of all neutron-optical aberration effects, they define the energy and momentum transfer dependent resolution function of the instrument. This method of ‘average’ values is very useful in the case of very sharp distributions (resolutions) or if no smaller errors than $\sim 10\%$ of the resolution-FWHM are required. The resolution function can be in many cases experimentally determined by performing calibration (e.g. vanadium) measurements.

However, the classical approach is not satisfying in many cases and represents only a first

* Corresponding author. Tel: +49-30-8062-3022; fax: +49-30-8062-2523.

E-mail address: zsigmond@hmi.de (G. Zsigmond).

approximation of data evaluation. Here are few examples:

- (1) in a wide range of momentum and energy transfers the resolution function is unknown, thus a separation of instrumental and physical/sample effects is not achievable;
- (2) a deconvolution of the resolution from the raw data is not always possible, e.g. in the range of broad peaks where the resolution is energy and/or momentum transfer dependent;
- (3) by neglecting the (poor) angular resolution, a re-binning/transforming of constant angle spectra into constant momentum spectra is unrealistic;
- (4) without back-tracing of particular neutron velocities/trajectories, a correct energy scale cannot be obtained – a simple energy shift is not precise for wide spectra because the time to energy transformation is non-linear.

Such difficulties can be overcome by performing three-dimensional (3D) real-geometry and real-physics Monte Carlo simulations including a detailed space-time distribution from the moderator. With the example of the high-resolution and wide dynamic range spectrometer IRIS [1] at ISIS, it will be shown that the inelastic resolution function can be computed with a good precision which is only limited by the statistical errors of the vanadium data used in the bench marking. Additionally, a Monte Carlo analysis/back-tracing of the instrumental effects helps to better extract the useful information lying in the experimental data [2,3]. The computing programmes could also be applied for instrument calculations aiming at the improvement of the time-of-flight backscattering technique [2,4].

One main component of neutron spectrometers can be a crystal monochromator/analyser. A realistic programming of these modules is decisive for the outgoing data because these complex instrument parts highly determine both the wavelength selection and incident/scattered intensities. The reflected neutron trajectories are sensitive on the d -spacing distribution and on the two-dimensional (2D) (taking only atomic/diffraction planes) mosaicity of the crystal. Both intensity and beam divergence are highly influenced by the focussing geometry of the monochromator or analyser.

The aim of the paper is to present recent results of the Monte Carlo study of the crystal analyser time-of-flight spectrometer IRIS underlining the performance of the crystal analyser MC code of VITESS, the Virtual Instrument Tool for ESS.

2. Simulation of crystal monochromators/analysers with VITESS

VITESS simulates the performance of instruments at continuous and pulsed neutron sources and it was primarily developed to support the ESS project. Introducing information can be read in Refs. [5–7]. Parts of the IRIS MC simulation programme of Zsigmond [2] as the crystal analyser, the inelastic sample and the inelastic evaluation codes were applied and generalised in the novel VITESS software.

The “crystal” module simulates a neutron monochromator or analyser (M/A) as a flat rectangular crystal or a matrix of flat crystal elements (CE-s) forming a focussing geometry. In all available options (1, flat-crystal; 2, wavelength-focussing-geometry; 3, external focussing- geometry-data) the reflecting surface of the CE is (h, k, l) oriented, i.e. it is parallel to the (h, k, l) crystal planes. The crystal structure can be characterised by setting the parameters d -spacing, d -spread, 2D mosaicity and reflectivity. The internal functions used to approximate probability distributions were defined as

(1) 2D Gaussian mosaic distribution:

$$P_m(\psi, \xi) = \exp(-\psi^2/2\sigma^2), \quad \text{with} \\ 1/\sigma^2 = \cos^2\xi/\sigma_Y^2 + \sin^2\xi/\sigma_Z^2, \quad (1)$$

where ψ, ξ are the polar angular coordinates of the mosaic normal vector in the frame of the CE and $\sigma_{Y,Z} = \eta_{Y,Z}/(8 \ln 2)^{1/2}$ are the Gaussian standard deviations. $\eta_{Y,Z}$ represent the horizontal and vertical FWHM of the mosaic distribution.

(2) The Lorentzian type d -spacing distribution:

$$P(d) = \Delta d^2/(4(d - d_0)^2 + \Delta d^2), \quad (2)$$

where d_0 is the d -spacing most probable and $\Delta d = \text{FWHM}$. P_m is normalised to give $P_m(0,0) = 1$, to be independent of parameters. Similarly $P(d_0) = 1$. This allows for a more straightforward

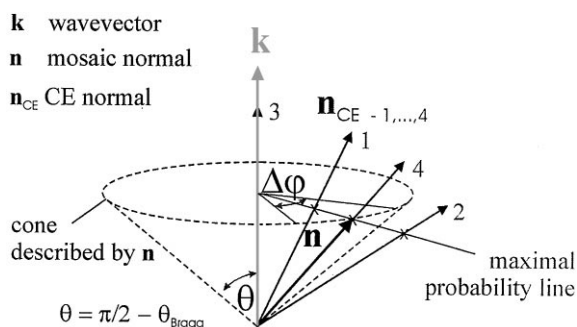


Fig. 1. The ‘Bragg-cone’: the reflecting mosaic piece normals describe a cone around the initial wavevector of the reflected neutron conforming to Bragg’s Law.

(self)control for the user and defines the maximal probability as equal to the reflectivity parameter.

In a first step, the CE hit by the neutron is searched in the CE-matrix. The neutron finds one mosaic piece of random d -spacing on which it is reflected. All possible orientations of the mosaic piece normals (determined by wavelength and d -spacing conforming to Bragg’s Law) describe a cone with an opening $\theta = \pi/2 - \theta_{\text{Bragg}}$, the actual axis being the initial wavevector of the neutron under consideration. In Fig. 1 the mosaic piece normal vector is labelled by \mathbf{n} and the normal vector of the CE by \mathbf{n}_{CE} . Fig. 1 shows the wavevector \mathbf{k} as fixed (in the frame of the neutron), that is, the individual neutrons see the CEs (\mathbf{n}_{CE} s) oriented in various directions labelled 1, ..., 4. Case 1 corresponds to the situation when \mathbf{n}_{CE} is inside the cone, 2 when outside, 3 when $\mathbf{n}_{\text{CE}} \parallel \mathbf{k}$ and 4 when $\mathbf{n}_{\text{CE}} \parallel \mathbf{n}$. The vectors \mathbf{k} and \mathbf{n} are approximately lying in the main plane of reflection. In the simple situation $\eta_Y = \eta_Z$, the most probable mosaic orientation is when \mathbf{k} , \mathbf{n} and \mathbf{n}_{CE} are co-planar vectors, i.e. they cross the ‘maximal probability line’ defined by the cross-points with the flat base of the cone. This is because in this case the angle between \mathbf{n} and \mathbf{n}_{CE} is minimal. For larger angles the probability decreases very rapidly as a function of the horizontal and vertical FWHM-s (in the input frame) of the mosaic distribution. Consequently, it is more economical to take for the random orientation of the mosaic pieces a finite interval $\Delta\varphi$ close to the maximal probability line. $\Delta\varphi$ must be large enough to

cover the Gaussian distribution in a reasonable definition range (including the tails). In the general case $\eta_Y \neq \eta_Z$, the minimum angle between \mathbf{n} and \mathbf{n}_{CE} does not mean automatically maximum probability in the distribution; however it well defines the centre of the angular range $\Delta\varphi$ (see if neutron \mathbf{k} vector parallel to beam axes). In the extreme case 3 (exact backscattering), it must be set $\Delta\varphi = 2\pi$ even if the mosaicity is very small in one of the directions, because of the computing algorithm (then by definition \mathbf{k} , \mathbf{n} and \mathbf{n}_{CE} are always coplanar). In case 4, $\Delta\varphi = 0$ yields $P = P_{\text{Max}} = \text{Reflectivity}$.

In the output, the new probability weight per neutron contains the product of the d -spacing and mosaic distributions of the CEs. The new coordinates of the neutron are computed consecutively by taking into account the exact orientation of the randomly selected reflecting mosaic piece. This precise trajectory calculation for each single neutron supplies the real correlation between mosaicity and reflected beam divergence. No transmission and multiple Bragg reflections are computed in the actual version. The detailed computation procedures of the module ‘crystal’ lead to a sufficient description of the factors which influence the resolution behaviour of the whole instrument. For reliable intensity comparisons between different types of instruments it might be necessary to renormalise with the ratio between intensities of measured and simulated calibration data.

An important output, the wavelength distribution for the PG(002) analyser array of IRIS is shown in Fig. 2. It can be observed that the lineshape is very close to the Lorentzian fitted, as this is expected for a PG(002) analyser in backscattering geometry with an effective $\Delta d/d \sim 0.002$ and mosaicity 0.8° . In this case the wavelength selection is dominated by the effective d -spacing distribution, which – by comparisons to measured data – was deduced to be Lorentzian. This direct wavelength monitoring is only possible in a simulation not in an experiment. However, the possibility in the MC simulations to separately monitor the distribution of one of the neutron coordinates (position, flight time, velocity vectors) helps to better understand the instrument optics.

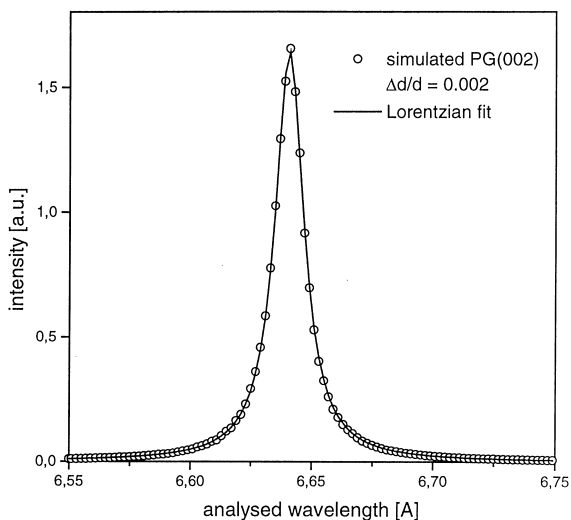


Fig. 2. The simulated wavelength resolution of the PG(002) backscattering analyser of IRIS can be well fitted with a Lorentzian – resembling the shape of the d -spacing distribution.

3. Simulation of IRIS

A detailed discussion of the crystal analyser spectrometer IRIS can be read in Refs. [1,2]. Here we will focus on the decisive factors determining the elastic and inelastic energy resolution of this neutron instrument: the moderator pulse and d -spread of the PG(002) backscattering analysers.

The used pulseshape coming from the liquid hydrogen moderator is a semi-empiric analytical assumption introduced in Ref. [2] relying on measured and MC simulated data of liquid hydrogen moderators [8]. The general expression applied for the time distribution was

$$p(t) = [1 - a_1 \exp(-t^2/\tau_1^2) + a_2 \exp(-t^2/\tau_2^2)] \times \exp(-t/\tau_{1n}). \quad (3)$$

The coefficients $a_{1,2}$ and $\tau_{1,2}$ determine the sharpness of the signal (see Fig. 8) and are energy dependent. It is known from moderator calculations that the time distribution of late neutrons shows an exponentially decaying tail characterised by τ_{1n} . Consistently, the first multiplication term in Eq. (3) is close to 1, when $t \gg \max[\tau_1, \tau_2]$. The distribution $p(t)$ was analysed in detail in order to

find out how much influence it has on the shape of the simulated elastic resolution. From fitting with $p(t)$ of the moderator pulse – which was numerically matched to give the correct vanadium spectra – resulted that the best fit can be obtained with $a_1 = 2$ and $a_2 = 1$. Additionally, fits proved that the number of parameters can be reduced by choosing $\tau_1 = \tau_2$ (58 μ s IRIS), without a significant change of the simulated signal shape in the detector. Consequently, the analytical form could be simplified to

$$p(t) = [1 - \exp(-t^2/\tau^2)] \times \exp(-t/\tau_{1n}). \quad (4)$$

A good agreement between the simulated elastic resolution lineshape and the vanadium measurement was obtained when the time constants and crystal analyser parameters were chosen as the estimations in Ref. [1]. The time constants were fine-tuned by minimising the quadratic deviation of the experimental vanadium and MC data. (To do this, the vanadium as well as the simulated counts per channel were first normalised to give the same peak integral.) The same procedure was used to adjust the average d -spacing of the PG(002) crystal analysers and the d -spread FWHM.

The d -spacing had to be adjusted at the known geometrical instrument parameters (flight path, etc.) in order to calibrate the energy transfer scale. From simulation of the elastic resolution it could be concluded that an exact energy scale cannot be directly calculated by only using the vanadium peak position and the kinetical formulas for IRIS. The asymmetry of the moderator pulse causes a small ~ 25 – 30μ s positive shift in the time of flight (3 detector time channels = 2μ eV at zero energy transfer) relative to an ideal delta-function moderator pulse. On the other hand, only the average velocity component parallel to the beam axis can be calculated from the position of the vanadium peak in the time-of-flight spectra. The calculation of the d -spacing of the analyser from the wavelength (according to the Bragg condition) requires however the knowledge of the absolute value of the velocity. The deviation as caused by the beam divergence was estimated by the simulation as 7μ s, i.e. ~ 1 time channel.

The d -spread $\Delta d/d$ was defined as the FWHM of the d -spacing distribution in the PG(002) crystal.

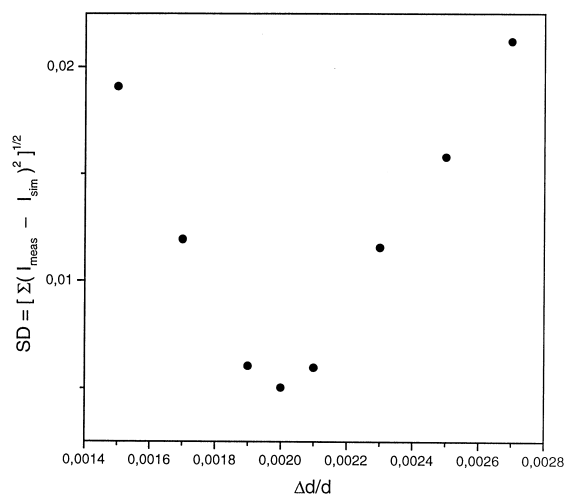


Fig. 3. Quadratic deviation between the measured and computed data showing the sensitivity on the adjusted parameter ($\Delta d/d$).

Comparing simulation results with vanadium calibration data, it could be concluded that distributions close to a Gaussian give to small intensity in the wings of the signal and the distribution of d is closer to a Lorentzian. The $\Delta d/d$ was fine-tuned in the range 0.0017–0.0025. In Fig. 3 the quadratic deviations between the measured and computed data are given showing the sensitivity on the adjusted parameter. The deviations between experimental and calculated vanadium intensities were summed up over all time channels.

The elastic energy resolution versus $\Delta d/d$ is shown in Fig. 4. The vanadium and the simulated lines were normalised to unity, thus the amplitudes of the signals strongly correlate with the FWHM of the peaks. The shown value $\Delta d/d = 2.1 \times 10^{-3}$ gives the closest match to the experimental data (MC – open circles). This high value represents an effective $\Delta d/d$, because we are measuring a large number of crystal elements in the analyser array at the same time, that is, the obtained $\Delta d/d$ is strongly influenced by the spread in the most probable d -spacing of the CEs. By setting the moderator time-pulse width zero (δ -signal), the “secondary” resolution FWHM was estimated as $\sim 10 \mu\text{eV}$. The broadening of the elastic line (the difference in the time of flight) is due to the neutrons flying with different velocities.

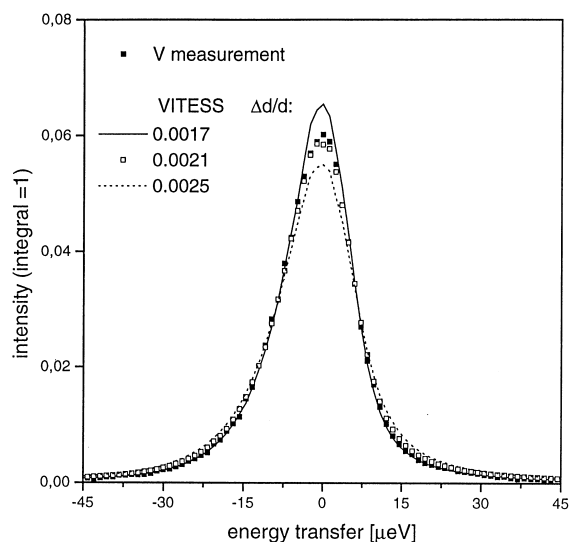


Fig. 4. The simulated elastic energy resolution versus $\Delta d/d$ as labelled by the continuous and dotted line and open squares. The experimental data are labelled by the full squares.

The bench marking of the MC simulation was completed by the elastic calibration presented above. Measurements on the “standard” liquid ^4He can be performed below 1 K to calibrate the energy scale of neutron spectrometers, which cover a compatible domain in the q - ω plane. It is another characteristic property of superfluid ^4He , that the single-excitation FWHM changes very little below 1 K and is of the order of magnitude $1 \mu\text{eV}$. This value is less than the conventional resolution performance of neutron instruments, and thus, the resolution can be obtained at the roton energy with a precision of μeV by measuring the linewidth below 1 K [9].

Therefore, the consecutive simulation at the roton energy represented the check for the bench marking performed. The form of the inelastic resolution of the instrument as shown in Fig. 5 is well defined by the suitable statistics of the neutrons collected in MC simulations. As it can be observed, there is a very good match between the measured and simulated data.

The inelastic lines are much more asymmetric (see below) and this is caused by the shape of the moderator pulse. The Lorentzian-like shape of the lines is due to the broadening of the signal during

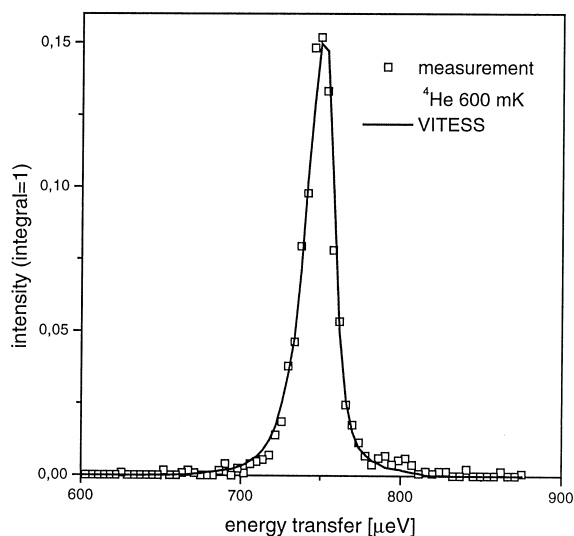


Fig. 5. Measured and simulated roton excitation lines at 600 mK – equivalent to the energy resolution at the roton peak position.

the time of flight, because the neutrons travel at different velocities, the wavelength band being selected by the crystal analysers of a Lorentzian-like d -spread. Since the analyser wavelength is directly proportional to the d -spacing (Bragg condition) and the time of flight is linear to the wavelength, the lineshape of the measured signal also resembles the distribution function of the d -spacing. This correspondence in shapes gives the reference for the choice of the d distribution in the crystal analyser module used in the calculation.

MC simulations were performed in order to calculate the energy-transfer-dependent energy resolution of the IRIS spectrometer in a wide range from 200 to 3000 μeV . The resulting spectrum is shown in Fig. 6. A set of $\text{FWHM}_{\text{intrinsic}} = 1 \mu\text{eV}$ Lorentzian lines (with no energy dispersion) was considered in the calculations. The interval between the signals was set to 250 μeV . The counts were ‘collected’ in 20 μs channels in order to optimise the computing time as well as the statistical spread. The instrumental line-broadening increases with increasing energy transfer. At the elastic position the energy resolution of IRIS amounts to 14.6 μeV . The FWHM of the resolution increases with increasing energy transfers: 22.2 μeV at 1 meV and

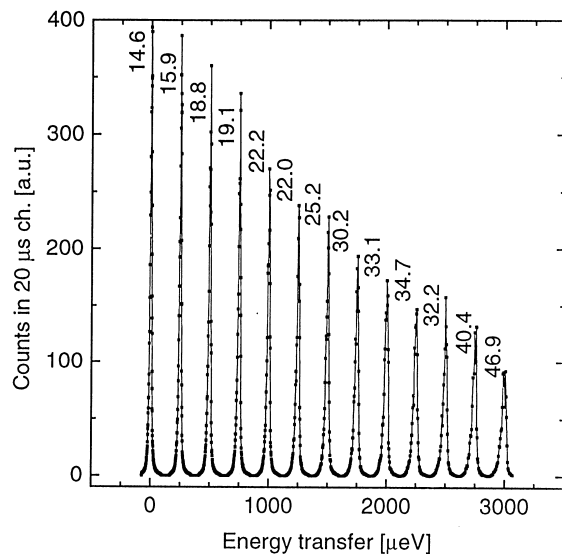


Fig. 6. Simulation of the inelastic energy resolution of IRIS as a function of the energy transfer.

46.9 μeV at 3 meV. The increase of the FWHM of the instrumental resolution at higher energy transfers can be explained by the equations used to transform time of flight into energy scale. It is worth noting that, while the FWHM of the energy resolution increases, the FWHM of the time resolution decreases with higher energy transfers. This is caused by the non-linear character of the relation between the flight time and the energy transfer.

The higher asymmetry in the inelastic peaks results from the higher energy transfer needed to create excitations: A higher energy transfer requires smaller incoming neutron wavelengths prior to the scattering, since the final energy is fixed by the analyser. The analyser crystal also determines the narrow wavelength bands $\Delta\lambda_{\text{PG}}$ (see Fig. 2) and $\Delta\lambda_{\text{inc}}$, which in the case of a delta-function scattering law are related to the incoming λ_{inc} by

$$\Delta\lambda_{\text{inc}} = \frac{\Delta\lambda_{\text{PG}}}{\lambda_{\text{PG}}^3} \times \lambda_{\text{inc}}^3 \quad (5)$$

as it can be obtained from the conservation of energy. It shows that the wavelength window gets smaller by the power of 3 with smaller incoming wavelengths. Thus, for larger energy transfers, the

smearing of the moderator time pulse is less significant, i.e. the asymmetry of the signal is preserved. The time-of-flight spectrum of the inelastic scan, where the time-resolution FWHM (μs) decreases with larger energy transfers, shows this instrumental effect. The decrease of the signal amplitude is mainly due to the factor k_f/k_i in the scattering probability.

It has to be mentioned here that the source pulse length was approximated independent of λ , which is not anymore exact for short wavelength. The LH2 moderator on ISIS generates pulses with 22λ (\AA) near the peak of the Maxwellian ($\sim 2.5 \text{\AA}$), while at longer wavelengths ($> 6 \text{\AA}$) the width is approximatively constant [1]. Similar calculations were done at LANSCE [10].

4. Application I: MC data reduction (MCDR)

The main importance of MC simulations consists in the possibility to develop a more precise numerical technique of data reduction beside the conventional ones.

As shown above, MC simulations can be used to calculate the exact instrumental resolution shape of the IRIS instrument. The inelastic energy resolution can be calculated in the full range of energy transfers. For a sharp Lorentzian-like excitation signal the FWHM can be approached by subtracting the FWHM value of the resolution from the experimental FWHM of the line. This procedure is considered as a first approach (I). However, it is not exact if there are important deviations from the Lorentzian shape for both the intrinsic line and the instrumental resolution. A next more exact approximation (II) simulates model scattering functions. A scan of the intrinsic linewidth, for example, can be performed in a wider range around the most probable value.

By minimising the quadratic deviation of the MC and measured spectra, the best values for the intrinsic parameters can be determined, for example,

$$\frac{\partial(\chi^2)}{\partial P_i} = \frac{\partial}{\partial P_i} \left[\sum_{\text{channels}} (I_{\text{meas}} - I_{\text{MC}}(P_1, \dots, P_6))^2 \right] = 0 \quad (6)$$

where P_i represent the parameters $\omega_{1,2}$, $\Gamma_{1,2}$, $A_{1,2}$ for two Lorentzians, I_{meas} represents the experimental counts per channel, and I_{MC} the counts computed. (Both measured and simulated intensities have to be normalised to the same integral to be able to make a comparison.) In an ideal case, where extremely long computing time is available, the procedure could be done by iteration. This means, in order to calculate the absolute minimum of the function χ of the six variables, the scanning procedure would need to be repeated many times in a large volume of the (P_1, \dots, P_6) configuration space until

$$d(\chi^2) = \sum_i \frac{\partial(\chi^2)}{\partial P_i} dP_i = 0, \quad (7)$$

where dP_i represent scanning steps. This general formulation results from the fact that χ^2 is analogous to a potential function and allows for confinements like $\Gamma_1 = \Gamma_1(\omega_1)$.

However, in practice such a long procedure can be avoided by using first the approach I, i.e. by scanning the parameters as close as possible to the most probable values. MC calculations show that in this case χ is minimised in a satisfying way by one parameter scans (such as ω_1 or Γ_1 scanned and the rest fixed) and that the adjustment can be done independently for each parameter. It is important to adjust those parameters first for which the quadratic deviation is most sensitive.

Here we illustrate how the intrinsic FWHM of the sharp roton peak was determined at 0.4 bars and 1.4 K by approach II of MCDR. The response function was modelled by a sum of two Lorentzians, including the q -dependence. The calculation of χ was performed by scanning the intrinsic linewidth in the range 30–57 μeV and normalising in the sharp peak. Some of the resulting signals are shown in Fig. 7. With a parabolic fit the minimum of the quadratic deviation could be calculated by using only a set of 6 values for the simulations of the intrinsic linewidth. The corresponding FWHM_i was found to be $43 \pm 5 \mu\text{eV}$. The determination error depends on the statistical spread of the counts in each channel for both the experimental and MC data.

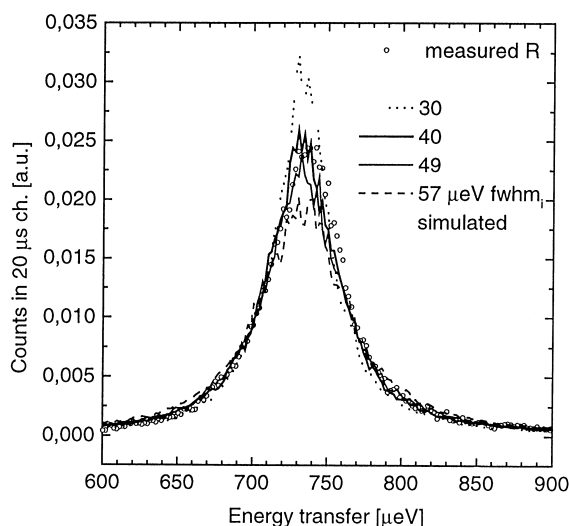


Fig. 7. Determination of the excitation FWHM by minimising the quadratic deviation between the computed and experimental spectra.

It is an important feature of the method presented here that constant angle spectra were simulated – by applying a model function in the sample module for the scattering law $S(\mathbf{q}, \omega)$ in function of momentum and energy transfer – and consecutively directly compared to the experimental ones. By tuning the model parameters, $S(\mathbf{q}, \omega)$ was directly obtained, without rebinning the spectra from constant angle to constant momentum and thereby the statistical errors were not increased.

5. Application II: instrument development

Not as in experimental data analysis where numerical computations of $S(\mathbf{q}, \omega)$ models are much more time-intensive, MC simulations already are an often implemented tool for neutron scattering instrument design or development.

A first question in building a new instrument is to choose the optimal moderator. The comparison of moderator performances is an important application of instrument design by means of computer simulations.

In Fig. 8 three time pulses resulting from different liquid-hydrogen moderators were plotted. The thin

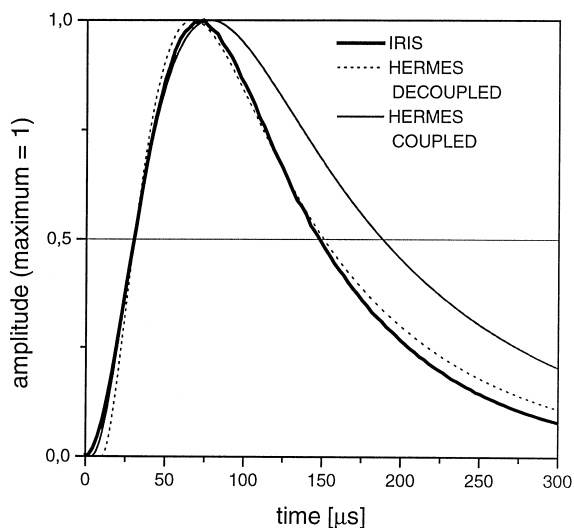


Fig. 8. Normalised time-pulses from different types of LH2 moderators for HERMES and IRIS.

continuous line represents (conforming to $p(t)$ in Section 3) the best fit to the measured pulse at 1.85 meV of the partially coupled moderator faced by FP9-11 at LANSCE. The dotted line is the best fit to the computed data of a decoupled version of the same moderator. The thick continuous line shows the pulse shape of the decoupled liquid-hydrogen moderator at the IRIS, deduced by bench-marking the simulation parameters in Refs. [2,3] and recently by VITESS relying on vanadium calibration data. The very close match of the two decoupled time pulses shows the consistency in the simulation method, starting with the choice of the analytical shape for the effective d -spacing distribution in the PG(002) analyser, up to the pulse function used for the time distribution in the source code.

In Fig. 9 the elastic energy resolution functions corresponding to the above mentioned time pulses were plotted by taking the same IRIS- or HERMES-type instrument set-up (with PG) in all three cases. (HERMES will use a partially coupled moderator and will have a geometrically optimised IRIS PG(002) set-up in phase I.) The decoupled versions give practically the same resolution FWHM $\sim 15 \mu\text{eV}$. It can be observed that the partially coupled moderator pulse offers an

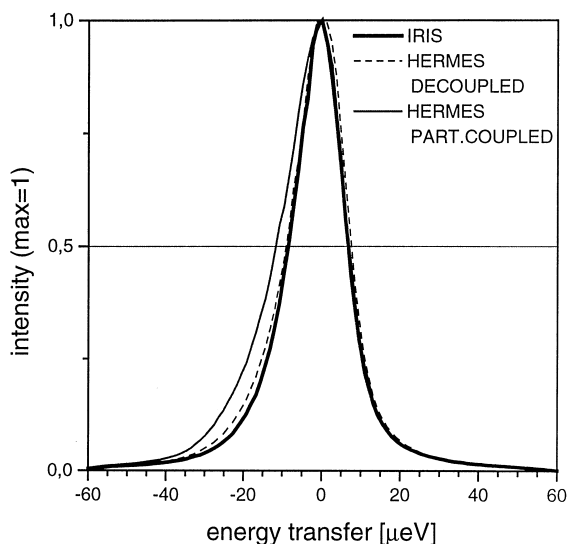


Fig. 9. The elastic IRIS/HERMES resolutions corresponding to the pulses in Fig. 8.

energy resolution FWHM larger by only $\sim 3 \mu\text{eV}$ compared to the decoupled one. However, moderator performance calculations show that in the partially coupled case the integral intensity of the pulse gives a gain of 2.5, which allows for a considerable improvement in the neutron statistics (run times of 5 h can be reduced to 2 h).

The time-of-flight backscattering technique in inelastic neutron scattering can further be improved [2,4]. The optimisation needed is to change flexibly the resolution of the instrument, energy transfer range and scattered intensity. At less intense, very sharp responses of a few μeV , a too large instrumental broadening can make the signal disappear in the instrumental background. Thus, fine structures in the spectrum cannot be revealed. Existing TOF-backscattering spectrometers like IRIS have a large dynamic range due to the inverted geometry (e.g. $0.4\text{--}3 \text{ \AA}^{-1}$, -0.2 to 3.5 meV) and can yield high elastic energy resolution of $15 \mu\text{eV}$ and high count rate at the same time. Backscattering spectrometers at reactors like IN10 (ILL) yield $\sim 1 \mu\text{eV}$ energy resolution and the dynamic range could be upgraded by temperature scan control of the monochromated neutrons to measure at energy transfers of $500 \mu\text{eV}$ in a range of $60 \mu\text{eV}$ [11].

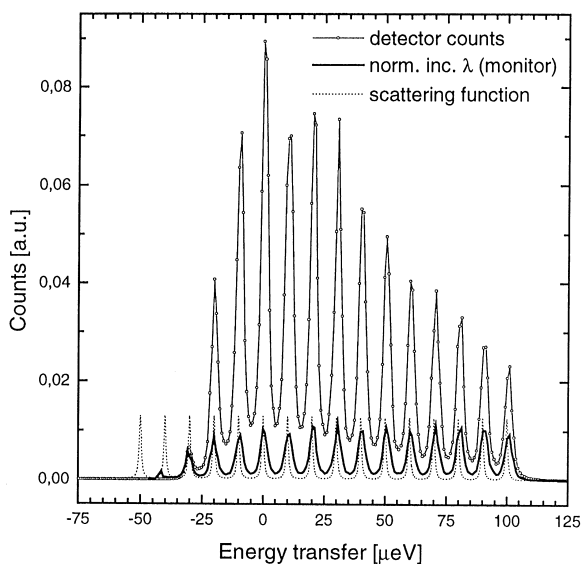


Fig. 10. Dynamic range of a fast-chopper Si(1 1 1) analyser spectrometer as illustrated by the simulation of a multippeak spectra.

The energy resolution can be improved by combining a Si(1 1 1) crystal analyser system and a fast-chopper modulated moderator pulse. In this case the intensity loss which is due to the absence of a mosaic structure and the narrow d -spread of Si(1 1 1) can be compensated for by large high-precision focusing geometries and bent crystal elements in order to optimise the resulting resolution and intensity [12].

In Fig. 10 a simulation result of a modulated pulse – Si(1 1 1) – analyser combination is presented. The instrument set-up is very similar to that of the IRIS TOF-backscattering spectrometer. Different from the IRIS instrument, the pulse from the LH2 moderator is modulated here by two counter-rotating fast-disc choppers operating at 250 Hz. The distance from the moderator to the fast choppers and the slit width determine, respectively, λ and the FWHM in TOF ($23.5 \mu\text{s}$) of the sharp signal cut out of the short pulse of the moderated neutrons of FWHM = $150 \mu\text{s}$. To achieve a better angular resolution, the secondary flight path was increased by setting the radius of the crystal analyser system to 2 m. The ‘eye-of-the needle’ convergent + divergent guide combination [13] was used to focus the neutrons from the moderator on the first fast-chopper

window and to increase the cross-section of the guide behind the fast choppers. A distance of 5.2 m from the moderator is an optimal position (taking into account the target shielding) for the modulating choppers for the wavelength of the Si backscattering analyser ($\sim 6.27 \text{ \AA}$).

Fig. 10 shows a scan of the inelastic scattering region. The intensity measured in the detector has a similar shape as the time pulse of the neutrons leaving the moderator. This can be explained by an ‘optical’ projection in the plane which can be defined by the flight path and the TOF of the neutrons, respectively. The short time-opening of the fast choppers determines a close relationship between the wavelength of the neutrons crossing the slit and the time as they leave the moderator surface.

6. Conclusions

It was demonstrated that Monte Carlo simulations can be used for resolution calculations of time-of-flight backscattering spectrometers in a wide dynamic range where experimental methods are not possible anymore. However, calibration results are necessary in the bench marking of the simulation method and in obtaining the input parameters. The good match between measured and simulated spectra shows that such numerical calculations are very exact and consistent with our knowledge on the dominant neutron-optical aberration effects produced by the instrument. The flexibility and general character of the VITESS modules used to ‘build’ the IRIS spectrometer makes us to conclude that the presented software can be generally implemented with similar success

for the computation of other neutron scattering instruments (see also Ref. [5]).

The bench marking of VITESS and rigorously checking of the computed results by means of experimental calibration data, allowed us the confidence to also implement it in the data reduction, in instrument design and development. Further calculations on the angular and momentum resolutions of crystal analyser spectrometers and on how these influence energy resolution and intensity of excitations in wide spectra are in progress.

References

- [1] C.J. Carlile, M.A. Adams, *Physica B* 182 (1992) 431.
- [2] G. Zsigmond, Ph.D. Thesis, Technische Universität Berlin, D83, Berlin, 1998.
- [3] G. Zsigmond, F. Mezei, Proceedings of the Second European Conference on Neutron Scattering, Budapest, Hungary, *Physica B* 276 (2000) 106.
- [4] F. Mezei, G. Zsigmond, Proceedings of the 14th Meeting of the International Collaboration on Advanced Neutron Sources, Starved Rock Lodge, IL, pp. 113–118.
- [5] D. Wechsler, G. Zsigmond, F. Streffer, F. Mezei, Proceedings of the Second European Conference on Neutron Scattering, Budapest, Hungary; *Physica B* 276 (2000) 71.
- [6] D. Wechsler, G. Zsigmond, F. Streffer, F. Mezei, *Neutron News* 11 (2000).
- [7] ViteSS Website: <http://www.hmi.de/projects/ess/viteSS>.
- [8] J.Z. Larese, L.L. Daemen, P.A. Seeger, J. Eckert, T.O. Brun, Proceedings of ICANS XIV, Starved Rock Lodge, IL, p. 586.
- [9] R. Crevecoeur, I. Schepper, L. Graaf, W. Montfrooij, E.C. Svensson, C.J. Carlile, *Nucl. Instr. Meth. A* 356 (1995) 415.
- [10] P.D. Ferguson, G.J. Russell, E. Pitcher, Proceedings of ICANS XIII, PSI, Villingen, 1995, p. 510.
- [11] J.C. Cook, W. Petry, A. Heidemann, J.-F. Barthelemy, *Nucl. Instr. Meth. A* 312 (1992) 553.
- [12] B. Frick, A. Magerl, Y. Blanc, R. Rebesco, *Physica B* 234–236 (1997) 1177.
- [13] F. Mezei, Proceedings of ICANS XII, 1993, pp. I-377.